frontiers | Frontiers in Energy Research

TYPE Original Research
PUBLISHED 04 October 2022
DOI 10.3389/fenrg.2022.991447

Check for updates

OPEN ACCESS

EDITED BY
Zbigniew Lodziana,
Polish Academy of Sciences, Poland

REVIEWED BY
Huai-Jun Lin,
Jinan University, China
Di Wan,
Norwegian University of Science and Technology, Norway

*CORRESPONDENCE
Claudia Zlotea,
claudia.zlotea@cnrs.fr

SPECIALTY SECTION
This article was submitted to Hydrogen Storage and Production, a section of the journal Frontiers in Energy Research

RECEIVED 11 July 2022
ACCEPTED 15 September 2022
PUBLISHED 04 October 2022

CITATION
Zlotea C, Bouzidi A, Montero J, Ek G and Sahlberg M (2022), Compositional effects on the hydrogen storage properties in a series of refractory high entropy alloys.
Front. Energy Res. 10:991447.
doi: 10.3389/fenrg.2022.991447

COPYRIGHT
© 2022 Zlotea, Bouzidi, Montero, Ek and Sahlberg. This is an open-access article distributed under the terms of the Creative Commons Attribution License (CC BY). The use, distribution or reproduction in other forums is permitted, provided the original author(s) and the copyright owner(s) are credited and that the original publication in this journal is cited, in accordance with accepted academic practice. No use, distribution or reproduction is permitted which does not comply with these terms.

Compositional effects on the hydrogen storage properties in a series of refractory high entropy alloys

Claudia Zlotea[1]*, Anis Bouzidi[1], Jorge Montero[1], Gustav Ek[2] and Martin Sahlberg[2]

[1]Univ Paris Est Creteil, CNRS, ICMPE, Thiais, France, [2]Department of Chemistry—Ångström Laboratory, Uppsala University, Uppsala, Sweden

The possible combinations in the multidimensional space of high entropy alloys are extremely broad, which makes the incremental experimental research limited. As a result, establishing trends with well-known empirical parameters (lattice distortion, valence electron concentration etc.) and predicting effects of the chemical composition change are vital to guide future research in the field of materials science. In this context, we propose a strategy to rationalize the effect of chemical composition change on the hydrogen sorption properties in a series of high entropy alloys: $Ti_{0.30}V_{0.25}Zr_{0.10}Nb_{0.25}M_{0.10}$ with *M* = Mg, Al, Cr, Mn, Fe, Co, Ni, Cu, Zn, Mo, Ta and ∅ (corresponding quaternary alloy). All materials are *bcc* alloys and absorb hydrogen at room temperature forming *fcc* or pseudo-*fcc* dihydride phases. The maximum hydrogen storage capacity at room temperature strongly depends on the valence electron concentration (VEC) of the alloys: the capacity is high (1.5–2.0 H/*M*) for low values of VEC (<4.9) whereas, a drastic fading is observed for VEC ≥4.9 which is the case for alloys with *M* being a late 3*d* transition metal. The structural analysis suggests that steric effects might not be responsible for this trend and electronic reasons may be invoked. Increasing the VEC by alloying with late 3*d* transition metals will fill the unoccupied valence states and the electrons from interstitial hydrogens can no longer be accommodated, which is unfavorable for hydrogen storage. Moreover, the onset temperature of desorption increases almost linearly with VEC for this composition series. These findings suggest that alloys with low VEC are more likely to become promising candidates for hydrogen storage.

KEYWORDS

high entropy alloys, hydrogen storage, chemical composition, valence electron concentration, lattice structure

Introduction

In the current environmental and energy context, hydrogen is considered a clean energy carrier able to achieve the decarbonization of the economy and to ensure a green and sustainable growth of industry (Spek et al., 2022). Among the challenges to be met in the development of decarbonized hydrogen economy (production, distribution, and transport, use ...) its compact, safe and efficient storage remains a technique to be developed for practical applications (Hirscher et al., 2020). To simultaneously meet these key criteria, the solid-state storage in the form of metal hydrides is a very promising method. Among the several types of materials forming hydrides currently under investigation, the so-called high-entropy alloys (HEA) have recently shown very interesting performances (Sahlberg et al., 2016; Nygård et al., 2020; Marques et al., 2021a; Ek et al., 2021; Witman et al., 2021; Lin et al., 2022).

The underlying principle of this class of alloy focuses on the exploration of the central region of the multicomponent phase diagram and is based on the mixing of five or more elements with near-equimolar concentrations (Miracle and Senkov, 2017). Several terms are commonly used to designate these materials: high-entropy alloys, multi-principal element alloys and multi-component alloys. It has been proposed to limit the denomination of high-entropy alloys to single-phase solid solutions (Miracle and Senkov, 2017). These alloys adopt simple crystal structures: body centered cubic - *bcc*, face centered cubic (cubic close-packed)—*fcc* and hexagonal close-packed—*hcp*. The stability of such phases seems to be based on several chemical and physical characteristics, such as configurational entropy, enthalpy of mixing, lattice distortion (δ) and valence electron concentration (VEC). The latter two empirical parameters have been previously defined in reference (Miracle and Senkov, 2017). Based on the analysis of experimental data it has been observed that single-phase HEAs typically have $\delta < 6.6\%$ (Yang and Zhang, 2012) and single-phase *bcc* alloys possess a VEC <6 whereas, single-phased *fcc* solid solutions can be found for VEC >7 (Couzinié and Dirras, 2019).

The study of reversible hydrogen absorption and desorption in these alloys is recent with a milestone in 2016 which marks the discovery of the *bcc* TiVZrNbHf alloy which can absorb important hydrogen amount (Sahlberg et al., 2016; Karlsson et al., 2018). This first study triggered a sustained research activity in the field already with several promising *bcc* alloys reported (Nygård et al., 2019a; Zlotea et al., 2019; Nygård et al., 2020; Witman et al., 2020; Marques et al., 2021b; Nygård et al., 2021; Witman et al., 2021). Most of these alloys contain refractory elements and quickly absorb hydrogen at room temperature forming *fcc* or pseudo-*fcc* (a slightly distorted *fcc*) dihydrides. Among these studies dedicated to *bcc* HEAs and their hydrogen storage properties several reports tackled systematic composition effect in order to rationalize their behavior toward hydrogen absorption/desorption. For example, Nygård et al. (2019a) firstly proposed to use VEC as a useful parameter to comprehend the evolution of several hydrogen sorption properties. It has been shown that the onset temperature for hydrogen desorption decreases linearly with the VEC while the volumetric expansion per metal atom from the *bcc* alloys to the *fcc* hydrides increases linearly with VEC. Recently, Ek et al. (2021) confirmed the latter growing trend of the unit cell volume expansion per metal atom by hydrogen absorption with VEC and also with the average Pauling electronegativities. Interestingly, a closely related parameter based on the volume per atom in a crystal was used as a descriptor to predict the thermodynamic stability of a wide range of metal hydrides by machine learning approach (Witman et al., 2020). However, proposing a clear trend of the hydrogen sorption properties with well-known parameters/descriptors is not trivial. This can be explained by the complexity of understanding chemical composition effects in alloys in which each element is highly concentrated and the distinction between main and minor elements is no longer relevant. Another difficulty is related to the vast compositional space of HEAs that has been sparingly explored for hydrogen storage purposes so far. Thus, providing a systematic and comprehensive assessment is restricted to a limited number of HEAs previously reported for the targeted application.

Recently, we have developed an original strategy based on the addition of 10 at% of a fifth element in an initial quaternary $Ti_{0.325}V_{0.275}Zr_{0.125}Nb_{0.275}$ alloy optimized for obtaining single-phase *bcc* alloy by various synthetic methods: arc melting and ball milling under inert atmosphere (Montero et al., 2019). This preliminary composition quickly absorbs hydrogen at room temperature and undergoes a phase transition from the initial *bcc* alloy to a *fcc* hydride phase (CaF_2-type structure) with a capacity of 1.75 H/M (2.5 wt%). The next step of our strategy implies the addition of 10 at% of a fifth element to the optimized pristine composition in order to obtain $Ti_{0.30}V_{0.25}Zr_{0.10}Nb_{0.25}M_{0.10}$ HEAs with various *M* elements (transition or lightweight metals). If five $Ti_{0.30}V_{0.25}Zr_{0.10}Nb_{0.25}M_{0.10}$ compositions have been already detailed in our earlier publications [*M* = Ta (Montero et al., 2020), Al (Montero et al., 2021a), Mg (Montero et al., 2021b), Mo (Bouzidi et al., 2021), and Cr (Bouzidi et al., 2022)], the present study aims to provide a comprehensive insight of a larger series of alloys including six other compositions with *M* = Mn, Fe, Co, Ni, Cu and Zn. This report will not duplicate our earlier results and discussion but will offer a global assessment of selected alloy's properties: storage capacity at room temperature, volume expansion upon full hydrogenation and onset temperature of desorption. Thus, a total of twelve materials, eleven quinary $Ti_{0.30}V_{0.25}Zr_{0.10}Nb_{0.25}M_{0.10}$ with *M* = Mg, Al, Cr, Mn, Fe, Co, Ni, Cu, Zn, Mo and Ta and one quaternary alloys, are presently studied and compared with the goal to track systematic effects on the hydrogen sorption properties due to changes in the chemical composition (10 at%).

Materials and methods

Depending on the nature of *M* element, the alloys $Ti_{0.30}V_{0.25}Zr_{0.10}Nb_{0.25}M_{0.10}$ were prepared, starting from high purity elements, either by high temperature arc melting or mechanochemistry. The alloys with *M* = Al, Cr, Mn, Mo and Ta were obtained by arc melting under 500 mbar Ar pressure (AM), as described previously (Montero et al., 2019; Montero et al., 2020; Montero et al., 2021a; Bouzidi et al., 2021), whereas the compositions with *M* = Mg, Fe, Co, Ni, Cu and Zn were synthesized by ball milling under 1 bar Ar atmosphere (BM). The BM process time varies between 45 and 120 min, depending on the composition. Alloys with *M* = Fe and Zn are formed after only 45 min of BM, whereas compositions with *M* = Co, Ni and Cu need slightly longer process time, *i.e.,* 60 min. The Mg-containing alloy is obtained after 120 min of ball milling, as explained in our earlier study (Montero et al., 2021b).

For the above-mentioned BM materials, the corresponding hydrides were synthesized by reactive ball milling (RBM) under 70 bar H_2 pressure during 120 min following the procedure reported elsewhere (Montero et al., 2019). For the sake of comparison, the quaternary $Ti_{0.325}V_{0.275}Zr_{0.125}Nb_{0.275}$ alloy was prepared by the three previous techniques *i.e.*, AM, BM and RBM (Montero et al., 2019). To ensure a fluid reading of the next sections, the quinary alloys will be identified either as Ti-V-Zr-Nb-*M* or simply by the *M*–containing element alloys whereas the quaternary composition will be called Ti-V-Zr-Nb.

Structural characterizations were carried out by X-ray powder diffraction (XRD) using both the laboratory D8 advance Bruker instrument (Cu K_α radiation λ = 1.5406 Å, Bragg- Brentano geometry) and the synchrotron radiation (SR-XRD) on the Cristal beamline (λ = 0.7289 Å) at SOLEIL large scale facility. For the SR-XRD investigations, the powder samples were placed in a capillary tube of 0.2 mm diameter. The scanning range was from 1° to 85° (2θ) within a 10-min acquisition time. Structural refinements of the XRD patterns were performed either by fundamental parameters approach as implemented in TOPAS (Cheary et al., 2004) or the Rietveld method (Rietveld, 1969) implemented in the Fullprof software (Rodríguez-Carvajal, 1993) (Thompson-Cox-Hastings pseudo-Voigt function for the peak shape).

Microstructural analyses were performed by scanning electron microscopy (SEM) acquiring back-scattered electron signal (BSE) using a Zeiss Merlin instrument. The samples (as coarse grains or powders) were embedded in an epoxy resin, then finely polished and finally coated with 1.5–2.5 nm Pd layer. The chemical mapping and quantitative chemical analyses of the samples were performed by energy dispersive X-ray spectroscopy (EDX).

The Pressure-Composition-Isotherms (PCI) were measured using the Sievert's method consisting of a manual homemade manometric device with thermostatically calibrated volumes, as detailed previously (Montero et al., 2019; Montero et al., 2020; Montero et al., 2021a; Bouzidi et al., 2021). The storage capacity was calculated using the real gas state equation for H_2 (GASPAK Version 3.32, Horizon Technologies). Prior to hydrogenation, the samples prepared by AM and RBM have been activated under dynamic vacuum at 350°C for 3–6 h or 400°C for 12 h, respectively. The choice of these values (350 and 400°C for AM and RBM materials, respectively) were justified by our previous results since RBM materials need slightly higher temperature to ensure full hydrogen desorption (Montero et al., 2019).

The hydrogen desorption was analyzed by thermal desorption spectroscopy (TDS) using a homemade instrument with a quadrupole mass spectrometer (QMS), as described elsewhere (Zlotea et al., 2011). The procedure consists of loading about 15 mg of the hydride sample and measuring the evolved gases by the QMS working under secondary vacuum (10^{-6} mbar) during constant heating with 1°C/min rate.

Results

The lattice distortion (δ) and VEC of the quinary $Ti_{0.30}V_{0.25}Zr_{0.10}Nb_{0.25}M_{0.10}$ alloys with *M* = Mg, Al, Cr, Mn, Fe, Co, Ni, Cu, Zn, Mo, and Ta as well as the starting quaternary composition, $Ti_{0.325}V_{0.275}Zr_{0.125}Nb_{0.275}$, are listed in Table 1. The values for the atomic radius for the lattice distortion calculation have been taken from the reference (SI Chemical Data, 1995).

The alloys with *M* = Al, Mn, Mo, and Ta together with the pristine quaternary composition prepared by AM are single-phased materials with *bcc* lattice, as proven by laboratory XRD in Figure 1A. The Cr-containing alloy also crystallizes in a *bcc* lattice with a small unknown impurity marked with star in Figure 1A.

The alloys with *M* = Mg, Fe, Co, Ni, Cu and Zn could only be obtained as *bcc* phases by using BM under Ar atmosphere due to several reasons. Firstly, the synthesis of Mg and Zn containing alloys by high temperature melting techniques is unsuitable due to the low melting point and high vapor pressure of these elements. Secondly, our attempts to prepare the Ti-V-Zr-Nb-*M* alloys with *M* = Fe, Co, Ni and Cu by AM were unsuccessful because of the formation of multiphase materials (see Supplementary Figure S1). High temperature melting seems to stabilize Laves phase intermetallics along with the desired *bcc* phase. Consequently, the BM technique is more suitable for the preparation of metastable *bcc* solid solutions, as proven by XRD during the BM process for the Ti-V-Zr-Nb-Fe alloy (Supplementary Figure S2). The XRD patterns of BM alloys are shown in Figure 1B. The diffraction peaks are broader than the AM alloys due to the small crystallite size and the numerous defects commonly introduced by the ball milling process. The *bcc* lattice parameters of the initial alloys are listed in Table 1.

Microstructural and chemical analyses by SEM/EDX clearly prove that all AM and RBM materials are single-phase alloys

TABLE 1 The synthetic method (arc melting-AM, ball milling under Ar-BM and reactive ball milling-RBM), the empirical parameters (δ and VEC), the lattice parameters of the initial and hydride phases, the capacity, and the onset temperature of desorption of the series of alloys $Ti_{0.30}V_{0.25}Zr_{0.10}Nb_{0.25}M_{0.10}$ alloys with *M* = Mg, Al, Cr, Mn, Fe, Co, Ni, Cu, Zn, Mo and Ta together with the initial quaternary composition.

M	Synthesis	δ (%)	VEC	Initial phase	a_{bcc} (Å)	Hydride phase	$a_{fcc/bct}$ (Å)	c_{bct} (Å)	Capacity (H/M)	T_{onset} (°C)
∅	AM	6.0	4.55	*bcc*	3.261 (1)	*fcc*	4.497 (1)	—	1.75	271
	BM				3.270 (1)		4.548 (1)	—	1.70	—
	RBM			—	—		4.474 (1)	—	1.75	—
Mg	BM, RBM	6.6	4.3	*bcc*	3.273 (1)	*fcc*	4.492 (1)	—	1.53	251
Al	AM	5.5	4.4	*bcc*	3.247 (1)	*bct*	3.137 (1)	4.374 (1)	1.60	114
Cr	AM	6.7	4.7	*bcc*	3.225 (1)	*fcc*	4.459 (1)	—	2.0	145
Mn	AM	5.7	4.8	*bcc*	3.267 (1)	*fcc*	4.482 (1)	—	2.0	195
Fe	BM, RBM	6.8	4.9	*bcc*	3.277 (4)	*fcc*	4.505 (3)	—	1.16	199
Co	BM	6.7	5.0	*bcc*	3.299 (8)	*fcc*	4.508 (3)	—	1.23	209
Ni	BM, RBM	6.7	5.1	*bcc*	3.296 (4)	*fcc*	4.500 (3)	—	1.1	218
Cu	BM, RBM	6.4	5.2	*bcc*	3.278 (4)	*fcc*	4.499 (1)	—	1.35	217
Zn	BM, RBM	5.9	5.3	*bcc*	3.279 (3)	*fcc*	4.506 (4)	—	1.18	228
Mo	AM	5.7	4.7	*bcc*	3.240 (3)	*fcc*	4.459 (1)	—	2.0	188
Ta	AM	5.5	4.6	*bcc*	3.263 (3)	*fcc*	4.474 (1)	—	2.0	125

(Supplementary Figure S3). Firstly, all AM alloys show a dendritic microstructure with a chemical gradient between the dendrites and interdendritic zones. This is due to the solidification process, as reported for many HEAs prepared by high temperature melting techniques (Zollinger and Fleury, 2020). More precisely, the dendrites are rich in Nb, whereas the interdendritic regions are poor in Nb which can be accounted by the distribution of the alloying elements in the liquid and the solid phases during solidification: a Nb-rich solid phase (dendrite) is firstly formed during solidification because of the higher melting temperature of Nb as compared to the other elements. Secondly, all RBM materials show a very homogenous composition without any secondary phase.

The hydrogen absorption properties have been determined by recording the PCI curves for both AM and RBM materials at room temperature (Figures 2A,B). This choice is motivated by our previous finding that alloys prepared by either AM or RBM show same hydrogen uptake whereas BM counterpart possesses a smaller capacity (Montero et al., 2019). Prior to hydrogenation investigation, the AM and RBM materials have been heat-treated at 350 and 400 °C under dynamic vacuum to ensure both the activation of AM alloys and the desorption of initial hydrogen from the RBM hydrides, respectively. The XRD patterns in Supplementary Figure S4 show that all desorbed materials are *bcc* single-phase which confirms the appropriateness of the pre-treatment.

All alloys quickly absorb hydrogen at 25°C with 90% of capacity reached in less than 5 min, as proven by the kinetic curves at room temperature under 25–30 bar H_2 pressure for a selection of materials in Supplementary Figure S5. Moreover, the alloys show similar PCI profile with a plateau-like feature at low pressure (the equilibrium pressure is below the gauge reading limit) followed by an ascendant branch at high pressure (Figure 2). This hints to a phase transition from the initial alloy toward a hydride phase at low pressure, irrespective of the composition. Moreover, very small solubility of hydrogen in the hydride phase is revealed. The maximum capacities vary from 1.1 to 2.0 H/*M* and seem to depend on the nature of *M*-type element despite its limited atomic concentration of only 10 at% (Table 1). Our previous finding put forward that for the same composition the AM and RBM prepared materials have similar capacities (Montero et al., 2019; Montero Banuelos, 2020). This hints that the chemical composition rather than the preparation method might be responsible for the observed variation of the capacity.

The XRD patterns of all hydrides are plotted in Figure 3: the hydrides of AM alloys have been investigated by SR-XRD whereas the hydrides prepared by RBM have been measured by laboratory XRD. Except Al- and Cr-containing alloys, all hydrides are single-phased *fcc* materials (CaF_2 type), in agreement with most of the reports on dihydrides of refractory HEAs (Zepon et al., 2018; Nygård et al., 2019b; Shen et al., 2019; Shen et al., 2020). The Al-containing hydride crystallizes into a body centered tetragonal (*bct*) structure that can be understood as a slightly distorted *fcc* lattice along *c*-axis, as also encountered in a small number of refractory HEAs (Sahlberg et al., 2016; Shen et al., 2020). The Cr-containing hydride adopts a *fcc* lattice with a small unknown impurity (marked as star in Figure 3A), as initially observed. The RBM hydrides show a broadening of the diffraction peaks as compared to AM materials because of the formation of large number of defects by mechanochemistry, as also noticed for the

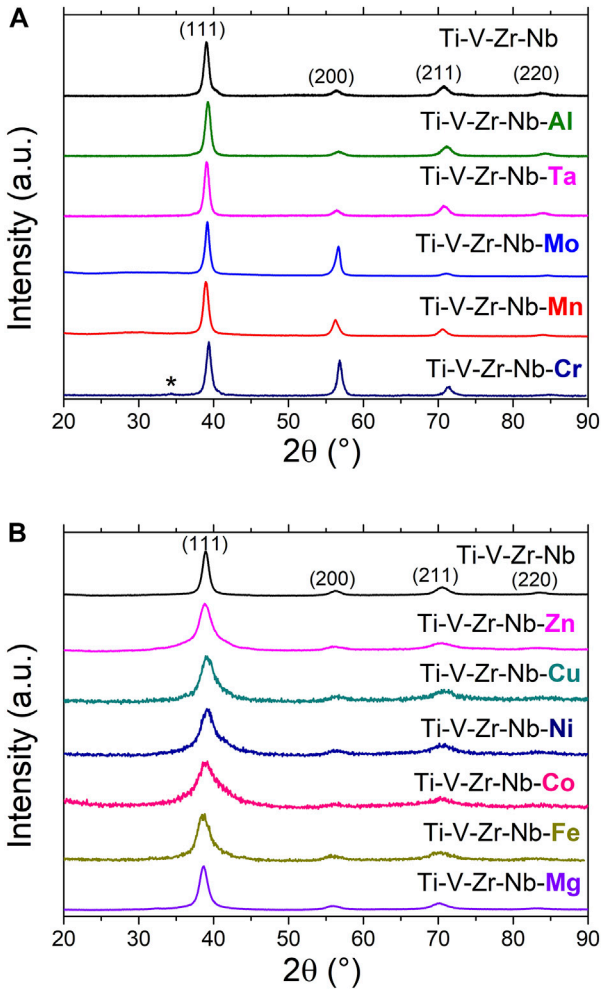

FIGURE 1
XRD patterns (λ = 1.5406 Å) of the $Ti_{0.30}V_{0.25}Zr_{0.10}Nb_{0.25}M_{0.10}$ alloys prepared by arc melting **(A)** and ball milling under inert gas **(B)**. The diffraction patterns of the starting quaternary alloy (Ti-V-Zr-Nb) as prepared by both methods are also shown.

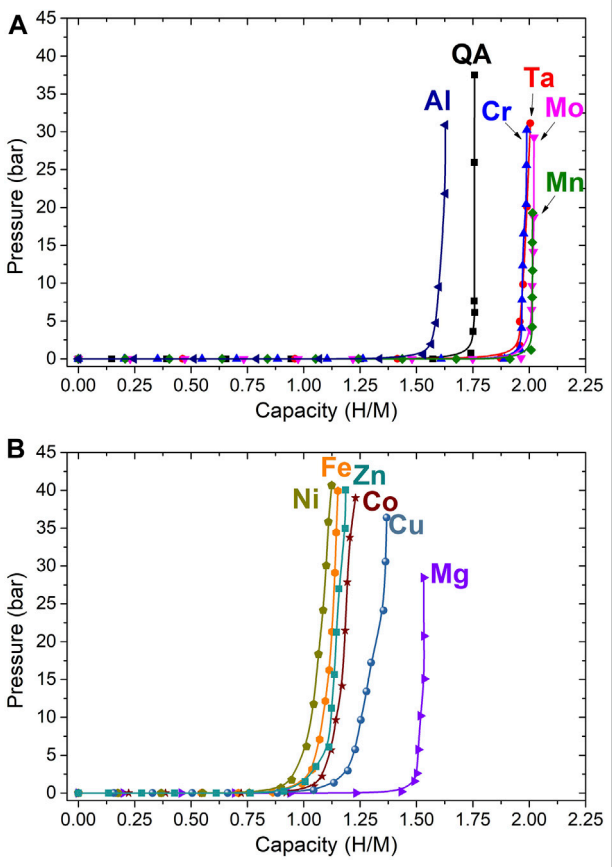

FIGURE 2
PCI curves at 25°C for arc melting alloys **(A)** and reactive ball milling compositions **(B)**. The PCI curve of the pristine quaternary alloy (QA) prepared by arc melting is also shown.

BM alloys in Figure 1B. The lattice parameters of the hydride phases are listed in Table 1.

The hydrogen desorption properties from all hydrides have been determined by thermo-desorption-spectroscopy with a heating rate of 1°C/min (Figure 4). The TDS profiles are strongly dependent on the type of *M* element, which also influences the values of the onset temperature of desorption and the temperature of the main peak corresponding to the maximum of the desorption rate. Most of the materials desorb hydrogen within one step (one main peak) whereas, two compositions stand apart with two step desorption *i.e.*, Al- and Ta-containing hydrides. Consequently, the latter alloys have the lowest onset desorption temperature among all studied materials. The onset temperature of desorption for all compositions are listed in Table 1.

Discussion

The eleven $Ti_{0.30}V_{0.25}Zr_{0.10}Nb_{0.25}M_{0.10}$ compositions with *M* = Mg, Al, Cr, Mn, Fe, Co, Ni, Cu, Zn, Mo, and Ta crystallize into a single-phase *bcc* lattice, as the pristine quaternary alloy (Montero et al., 2019). There is one exception for Cr-alloy which shows the presence of a small unknown impurity. One hypothesis to explain this finding is based on the lattice distortion parameter. Among the twelve alloys, only four compositions (*M* = Cr, Fe, Co and Ni) have a lattice distortion (δ) larger than 6.6% which is the empirical upper limit for obtaining solid solutions, as proposed in reference (Yang and Zhang, 2012). This might account for the presence of a small impurity in the case of Cr-containing alloy prepared by AM. The other three alloys (*M* = Fe, Co, and Ni) have been prepared by BM and consequently, the diffraction peaks are very broad making the identification of minor secondary phases challenging (Figure 1B).

Interestingly, the *bcc* lattice parameters, as determined by structural analysis, show a weak increasing tendency with the

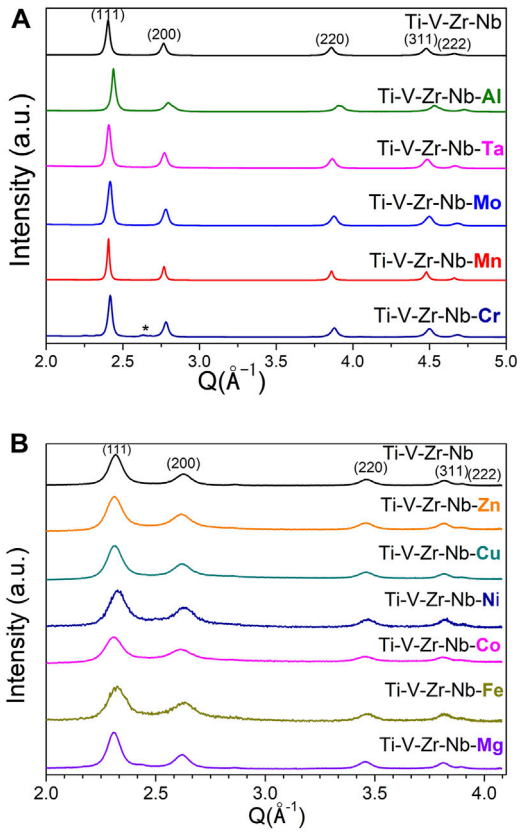

FIGURE 3
SR-XRD patterns of the hydrides of compositions prepared by arc melting **(A)** and laboratory XRD of the hydrides prepared by reactive ball milling **(B)**. For the sake of comparison, the quaternary hydrides prepared by hydrogenation of AM alloy and by RBM are also shown.

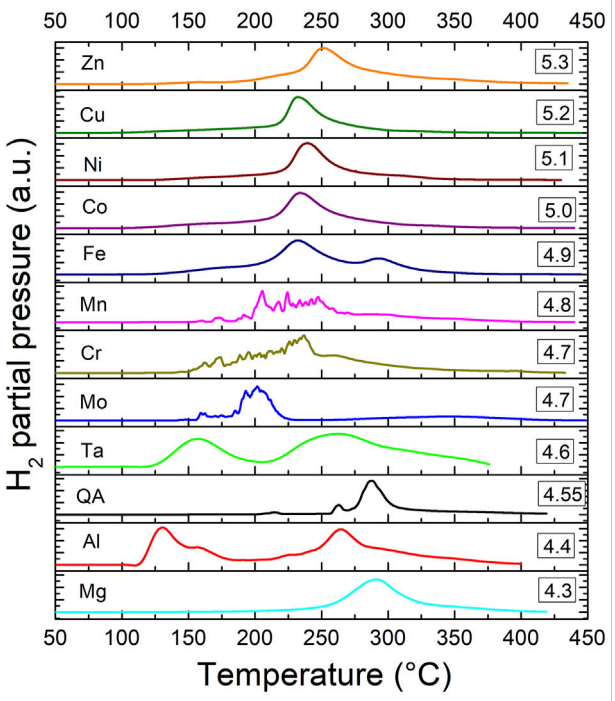

FIGURE 4
The TDS spectra for the hydrogen desorption from the $Ti_{0.30}V_{0.25}Zr_{0.10}Nb_{0.25}M_{0.10}$ alloys with *M* = Mg, Al, Cr, Mn, Fe, Co, Ni, Cu, Zn, Mo, and Ta. Quaternary alloy (QA) is also shown. The spectra are stacked as function of increasing VEC.

lattice distortion (Figure 5), with one exception for Cr-containing alloy that might be explained by the presence of a small impurity, as discussed above. Moreover, the attempts to correlate the *bcc* lattice parameters to other empirical parameters such as, the average atomic radius and VEC failed (Supplementary Figure S6).

The hydrogen storage capacities expressed as H/*M* are plotted against VEC in Figure 6A to highlight the effect of the nature of the *M* element on the hydrogen absorption performances. Obviously, two main groups of alloys can be distinguished: those with low VEC (<4.9) with a capacity in the range 1.5–2.0 H/*M* and the alloys with VEC ≥4.9 with low uptakes between 1.1–1.35 H/*M*. This trend is in line with previous results from a different series of refractory HEAs (Nygård et al., 2019a). In this article the trend has been accounted for a very high H_2 pressure necessary to ensure the phase transition to a hydride phase. In our case, the PCI curves of all materials are comparable indicating a phase transition to a *fcc* or pseudo-*fcc* (*bct*) hydride phase, irrespective of composition.

In order to better understand the evolution of the hydrogen absorption properties, the relative volume expansion per metal atom from the initial alloy to the related hydride phase was calculated, as initially proposed by Nygård et al. (2019a):

$$\alpha = \left[(V/Z)_{fcc} - (V/Z)_{bcc} \right] / (V/Z)_{bcc} \quad (1)$$

where *V* is the unit cell volume and *Z* is the number of metal atoms in the unit cell for *fcc* or *bcc* phases.

Figure 6B displays the relative volume expansion as a function of VEC for all considered alloys including the quaternary one. All materials show a relative volume expansion scattered between 0.25 and 0.320 with an average value at 0.29. Moreover, there is no clear correlation of this parameter with VEC which is in contrast with earlier findings showing a linear increase of α with VEC (Nygård et al., 2019a; Ek et al., 2021). However, if only AM alloys are considered (the red dotted square in Figure 6B), the correlation is closer to the previous linear trend reported by Ek et al. (2021) and Nygård et al. (2019a). Our result demonstrates that the volume expansion upon hydride formation is comparable among this series of alloys, irrespective of the hydrogen capacity and composition. To better discern steric effects, the volume of interstitial hydrogen atoms has been calculated from the cell volume

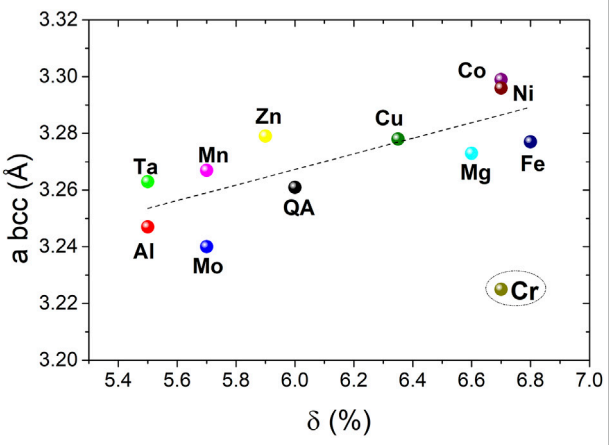

FIGURE 5
The *bcc* lattice parameters evolution with the lattice distortion for the series of the $Ti_{0.30}V_{0.25}Zr_{0.10}Nb_{0.25}M_{0.10}$ alloys with *M* = Mg, Al, Cr, Mn, Fe, Co, Ni, Cu, Zn, Mo, and Ta. QA designates the quaternary alloy whereas the quinary compositions are marked with the *M* element.

expansion per metal atom divided by the capacity as H/*M* in Figure 6C. Consistent with previous result, there are two groups of alloys depending on VEC. The alloys with VEC <4.9 show a volume of interstitial H in the range 2.5–3.2 Å^3 with an average value of 2.7 (2) Å^3, close to 2.9 Å^3 proposed by Peisl et al. (1978) for various metals and alloys. The compositions with VEC ≥4.9 have larger values of the volume of interstitial H (3.8 and 4.7 Å^3) that seems to indicate that H atoms occupy a larger average volume in the presence of late 3*d* transition metals. This hints to the hypothesis that steric effects such as, the available volume of interstitial sites, might not be responsible for the observed variation of hydrogen absorption capacity with composition.

Therefore, the decrease of the hydrogen capacity with increasing VEC might be accounted by electronic effects. In the simplest rigid *d* band model, interstitial hydrogen atoms will donate their unique electron to the unoccupied electronic states in the conduction band of the metal. Thus, increasing the VEC by alloying with late 3*d* transition metals will fill the unoccupied valence states to the extent that electrons from interstitial

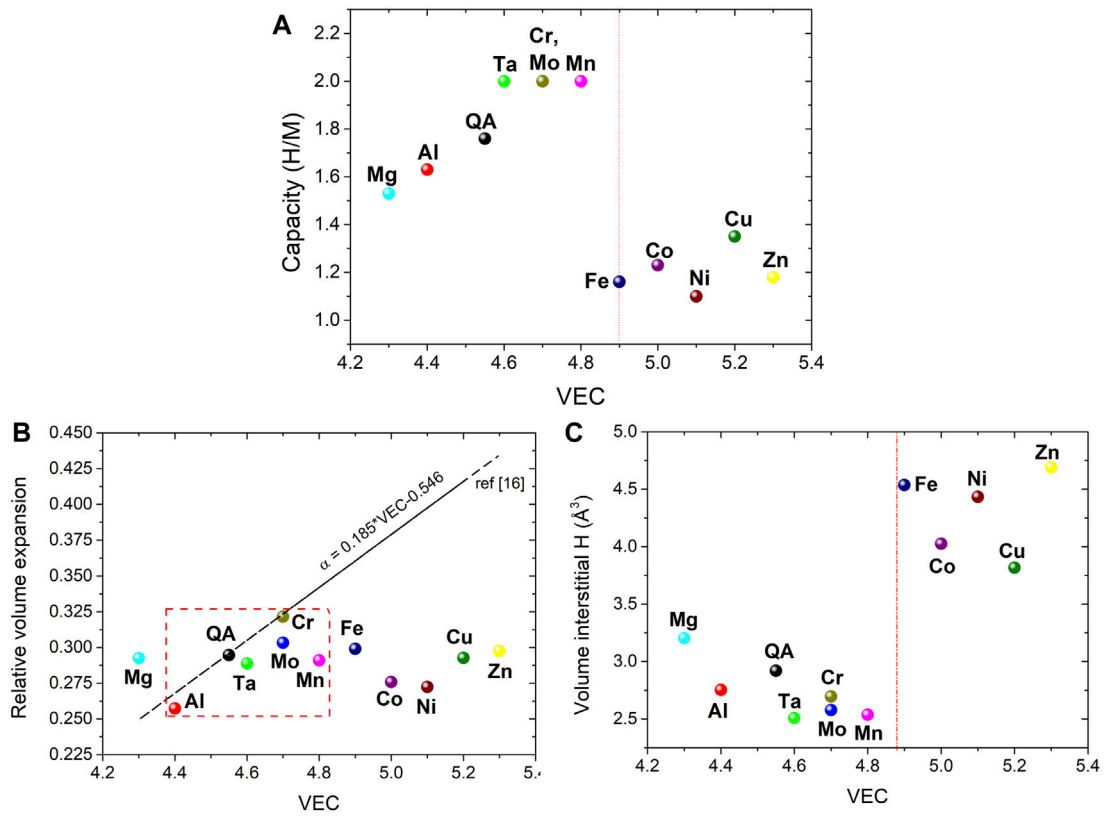

FIGURE 6
The hydrogen storage capacity **(A)**, the relative volume expansion per metal atom **(B)** and the volume of interstitial H **(C)** versus VEC for the series of the $Ti_{0.30}V_{0.25}Zr_{0.10}Nb_{0.25}M_{0.10}$ alloys with *M* = Al, Cr, Mn, Fe, Co, Ni, Cu, Zn, Mo, and Ta as well as the quaternary pristine alloy (QA). For comparison, the linear correlation proposed earlier by Nygård et al. (2019a) is also shown as dotted line in the B graphic. The red dotted square indicated the arc melting prepared materials.

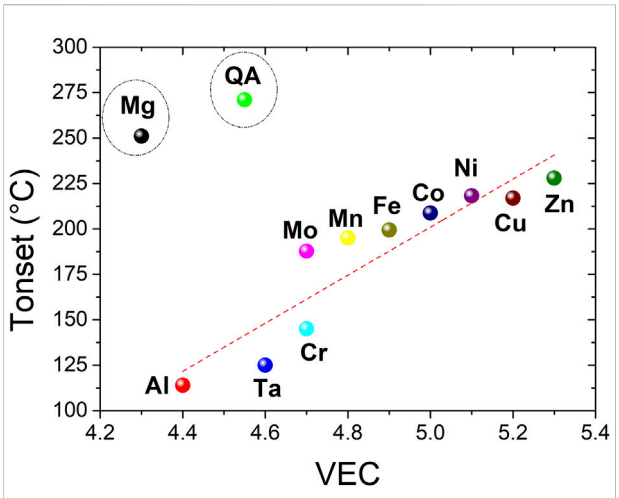

FIGURE 7
The variation of the onset temperature of desorption with VEC for the $Ti_{0.30}V_{0.25}Zr_{0.10}Nb_{0.25}M_{0.10}$ alloys with *M* = Mg, Al, Cr, Mn, Fe, Co, Ni, Cu, Zn, Mo, and Ta together with the quaternary material (QA).

hydrogens can no longer be accommodated. Consequently, increasing the VEC of the HEAs above 4.9 becomes unfavorable for hydrogen storage. Moreover, this value is in good agreement with the earlier suggestion for conventional *bcc* alloys. Lynch et al. (1978) and Kagawa et al. (1991) demonstrated that if the parameter electron per atom ratio (e/a) overpasses 5.0, the absorption capacity of V-Cr and V-Ti alloys strongly decreases.

The onset temperatures of desorption for the main peak, as determined by TDS, are plotted as function of VEC in Figure 7. Most of these values show an increasing linear correlation with VEC with two outliers, the quaternary pristine material, and the Mg-containing alloy. At this stage of our comprehension, we cannot explain the reason of this behavior. At a first glance, the addition of a fifth element in the initial material is beneficial since the onset temperature of desorption decreases for all quinary alloys, irrespective of composition, as compared to the pristine quaternary alloy.

The lowest desorption temperatures are obtained for Al- and Ta-containing alloys that also possess low VEC. For this series of compositions, it seems that low VEC is beneficial for both high hydrogen capacity and low onset desorption temperature.

Interestingly, the variation of the onset temperature of desorption was found to decrease with VEC in a previous study of a series of HEAs (Nygård et al., 2019a; Ek et al., 2021). However, the thermal analyses are based on different experimental conditions and measurement techniques (TDS under high vacuum in the present case and DSC under atmospheric pressure in the previous report).

To better comprehend this discrepancy, one suggestion would be to scrutinize the type of alloys chosen for constructing the statistics of materials pool. In the studies conducted by Nygård et al. (2019a) and Ek et al. (2021) several ternary, quaternary, and quinary HEAs have been selected containing exclusively refractory metals in the wide definition sense (Ti, V, Cr, Zr, Nb, Mo, Hf, and Ta). These alloys are mainly equimolar with only few of them non-equimolar. Thus, the alloy's pool comprises different types of alloys (from ternary to quinary) containing refractory elements. Here, the methodology is different: the starting point is a fixed quaternary alloy with optimized composition (non-equimolar) then, a fifth element of diverse type is added in limited quantity to form a total of eleven quinary systems. The change in composition in our case is limited (10 at%) but this allows to scan a broader range of additional atoms from light non-transition metals (Mg, Al) to the almost full range of 3*d* transition elements (from Cr to Zn) and several refractory ones (Mo and Ta). Therefore, we believe that this approach consistently tries to tackle effects of chemical composition change in high entropy alloys in order to advocate a statistical assessment and uncover interesting tendencies of hydrogen absorption with well-known empirical parameters.

Conclusion

In this report, we propose a novel methodology to rationalize the effect of the composition on the hydrogen sorption properties of a series of HEAs by altering only one element at a time contained in a limited quantity. It is shown that the hydrogen storage capacity strongly depends on VEC of the alloys: the capacity is high in the range 1.5–2.0 H/*M* for low VEC (<4.9) whereas, a fading is observed for VEC ≥4.9 corresponding to alloys with *M* being a late 3*d* transition metal. The structural analysis of hydrides suggests that steric effects might not be responsible for this trend. Consequently, increasing the VEC by alloying with late 3*d* transition metals will fill the unoccupied valence states and the electrons from interstitial hydrogens can no longer be accommodated decreasing the overall hydrogen storage capacity. Moreover, the onset temperature of desorption increases almost linearly with VEC for this composition series suggesting that HEAs with low VEC (<4.9) are more likely to become promising candidates for hydrogen storage.

Data availability statement

The original contributions presented in the study are included in the article/Supplementary Material, further inquiries can be directed to the corresponding author.

Author contributions

Conceptualization: CZ; formal analysis: AB and JM; investigation and methodology: AB, JM, GE, MS; supervision

and validation: CZ; writing original draft: CZ; writing—review and editing, AB, JM, GE, MS, and CZ.

Funding

This research was funded by ANR MASSHY project (ANR-19-CE05-0029-01) and NordForsk project "Neutrons for multi-funtional hydrides—FunHy" (project Nr. 81942).

Acknowledgments

CZ and AB acknowledge Valérie Lalanne and Loïc Perrière from ICMPE for help with arc melting. Benjamin Villeroy and Fermin Cuevas from ICMPE are acknowledged for assistance with ball milling. CZ and AB acknowledge Fabrice Couturas from ICMPE with help and assistance for hydrogenation measurements and Erik Elkaim for being the local contact during the XRD experiments on the CRISTAL beamline at SOLEIL synchrotron. GE and MS acknowledge financial support from NordForsk through the project "Neutrons for multi-funtional hydrides—FunHy" (project Nr. 81942).

Conflict of interest

The authors declare that the research was conducted in the absence of any commercial or financial relationships that could be construed as a potential conflict of interest.

Publisher's note

All claims expressed in this article are solely those of the authors and do not necessarily represent those of their affiliated organizations, or those of the publisher, the editors and the reviewers. Any product that may be evaluated in this article, or claim that may be made by its manufacturer, is not guaranteed or endorsed by the publisher.

Supplementary material

The Supplementary Material for this article can be found online at: https://www.frontiersin.org/articles/10.3389/fenrg.2022.991447/full#supplementary-material

References

Bouzidi, A., Laversenne, L., Nassif, V., Elkaim, E., and Zlotea, C. (2022). Hydrogen storage properties of a new Ti-V-Cr-Zr-Nb high entropy alloy. *Submitt Hydrog.* 3 (2), 270–284. doi:10.3390/hydrogen3020016

Bouzidi, A., Laversenne, L., Zepon, G., Vaughan, G., Nassif, V., and Zlotea, C. (2021). Hydrogen sorption properties of a novel refractory Ti-V-Zr-Nb-Mo high entropy alloy. *Hydrogen* 2 (4), 399–413. doi:10.3390/hydrogen2040022

Cheary, R. W., Coelho, A. A., and Cline, J. P. (2004). Fundamental parameters line profile fitting in laboratory diffractometers. *J. Res. Natl. Inst. Stand. Technol.* 109 (1), 1–25. doi:10.6028/jres.109.002

Couzinié, J. P., and Dirras, G. (2019). Body-centered cubic high-entropy alloys: From processing to underlying deformation mechanisms. *Mat. Charact.* 147, 533–544. doi:10.1016/j.matchar.2018.07.015

Ek, G., Nygård, M. M., Pavan, A. F., Montero, J., Henry, P. F., Sørby, M. H., et al. (2021). Elucidating the effects of the composition on hydrogen sorption in TiVZrNbHf-based high-entropy alloys. *Inorg. Chem.* 60 (2), 1124–1132. doi:10.1021/acs.inorgchem.0c03270

Hirscher, M., Yartys, V. A., Baricco, M., Bellosta von Colbe, J., Blanchard, D., Bowman, R. C., et al. (2020). Materials for hydrogen-based energy storage – past, recent progress and future outlook. *J. Alloys Compd.* 827, 153548. doi:10.1016/j.jallcom.2019.153548

Kagawa, A., Ono, E., Kusakabe, T., and Sakamoto, Y. (1991). Absorption of hydrogen by vanadium-rich V-Ti-based alloys. *J. Less Common Metals* 172–174, 64–70. doi:10.1016/0022-5088(91)90433-5

Karlsson, D., Ek, G., Cedervall, J., Zlotea, C., Møller, K. T., Hansen, T. C., et al. (2018). Structure and hydrogenation properties of a HfNbTiVZr high-entropy alloy. *Inorg. Chem.* 57 (4), 2103–2110. doi:10.1021/acs.inorgchem.7b03004

Lin, H. J., Lu, Y. S., Zhang, L. T., Liu, H. Z., Edalati, K., and Révész, Á. (2022). Recent advances in metastable alloys for hydrogen storage: A review. *Rare Met.* 41 (6), 1797–1817. doi:10.1007/s12598-021-01917-8

Lynch, J. F., Reilly, J. J., and Millot, F. (1978). The absorption of hydrogen by binary vanadium-chromium alloys. *J. Phys. Chem. Solids* 39 (8), 883–890. doi:10.1016/0022-3697(78)90150-6

Marques, F., Balcerzak, M., Winkelmann, F., Zepon, G., and Felderhoff, M. (2021). Review and outlook on high-entropy alloys for hydrogen storage. *Energy Environ. Sci.* 14 (10), 5191–5227. doi:10.1039/d1ee01543e

Marques, F., Balcerzak, M., Winkelmann, F., Zepon, G., and Felderhoff, M. (2021). *Review and outlook on high-entropy alloys for hydrogen storage*. Energy Environ Sci [Internet][cited 2021 Sep 24]; Available from: https://pubs.rsc.org/en/content/articlelanding/2021/ee/d1ee01543e.

Miracle, D. B., and Senkov, O. N. (2017). A critical review of high entropy alloys and related concepts. *Acta Mat.* 122, 448–511. doi:10.1016/j.actamat.2016.08.081

Montero Banuelos, J. (2020). *Refractory high entropy alloys for hydrogen storage*. [Internet] [Theses]. Université Paris-Est. Available from: https://tel.archives-ouvertes.fr/tel-03382754.

Montero, J., Ek, G., Laversenne, L., Nassif, V., Sahlberg, M., and Zlotea, C. (2021). How 10 at% Al addition in the Ti-V-Zr-Nb high-entropy alloy changes hydrogen sorption properties. *Mol. Basel Switz.* 26 (9), 2470. doi:10.3390/molecules26092470

Montero, J., Ek, G., Laversenne, L., Nassif, V., Zepon, G., Sahlberg, M., et al. (2020). Hydrogen storage properties of the refractory Ti–V–Zr–Nb–Ta multi-principal element alloy. *J. Alloys Compd.* 835, 155376. doi:10.1016/j.jallcom.2020.155376

Montero, J., Ek, G., Sahlberg, M., and Zlotea, C. (2021). Improving the hydrogen cycling properties by Mg addition in Ti-V-Zr-Nb refractory high entropy alloy. *Scr. Mat.* 194, 113699. doi:10.1016/j.scriptamat.2020.113699

Montero, J., Zlotea, C., Ek, G., Crivello, J. C., Laversenne, L., and Sahlberg, M. (2019). TiVZrNb multi-principal-element alloy: Synthesis optimization, structural, and hydrogen sorption properties. *Molecules* 24 (15), 2799. doi:10.3390/molecules24152799

Nygård, M. M., Ek, G., Karlsson, D., Sahlberg, M., Sørby, M. H., and Hauback, B. C. (2019). Hydrogen storage in high-entropy alloys with varying degree of local lattice strain. *Int. J. Hydrogen Energy* 44 (55), 29140–29149. doi:10.1016/j.ijhydene.2019.03.223

Nygård, M. M., Ek, G., Karlsson, D., Sørby, M. H., Sahlberg, M., and Hauback, B. C. (2019). Counting electrons - a new approach to tailor the hydrogen sorption properties of high-entropy alloys. *Acta Mat.* 175, 121–129. doi:10.1016/j.actamat.2019.06.002

Nygård, M. M., Fjellvåg, Ø. S., Sørby, M. H., Sakaki, K., Ikeda, K., Armstrong, J., et al. (2021). The average and local structure of TiVCrNbDx (x=0, 2.2, 8) from total scattering and neutron spectroscopy. *Acta Mat.* 205, 116496. doi:10.1016/j.actamat.2020.116496

Nygård, M. M., Sławiński, W. A., Ek, G., Sørby, M. H., Sahlberg, M., Keen, D. A., et al. (2020). Local order in high-entropy alloys and associated deuterides – A total scattering and reverse Monte Carlo study. *Acta Mat.* 199, 504–513. doi:10.1016/j.actamat.2020.08.045

Peisl, H. (1978). "Lattice strains due to hydrogen in metals," in *Hydrogen in metals I [internet]. Topics in applied physics*. Editors G. Alefeld and J. Völkl (Berlin, Heidelberg: Springer Berlin Heidelberg), 28. [cited 2020 Sep 4]. p. 53–74Available from: http://link.springer.com/10.1007/3540087052_42.

Rietveld, H. M. (1969). A profile refinement method for nuclear and magnetic structures. *J. Appl. Crystallogr.* 2 (2), 65–71. doi:10.1107/s0021889869006558

Rodríguez-Carvajal, J. (1993). Recent advances in magnetic structure determination by neutron powder diffraction. *Phys. B Condens. Matter* 192 (1), 55–69. doi:10.1016/0921-4526(93)90108-i

Sahlberg, M., Karlsson, D., Zlotea, C., and Jansson, U. (2016). Superior hydrogen storage in high entropy alloys. *Sci. Rep.* 6, 36770. doi:10.1038/srep36770

Shen, H., Hu, J., Li, P., Huang, G., Zhang, J., Zhang, J., et al. (2020). Compositional dependence of hydrogenation performance of Ti-Zr-Hf-Mo-Nb high-entropy alloys for hydrogen/tritium storage. *J. Mat. Sci. Technol.* 55, 116–125. doi:10.1016/j.jmst.2019.08.060

Shen, H., Zhang, J., Hu, J., Zhang, J., Mao, Y., Xiao, H., et al. (2019). A novel TiZrHfMoNb high-entropy alloy for solar thermal energy storage. *Nanomaterials* 9 (2), 248. doi:10.3390/nano9020248

SI chemical data, third edition (aylward, gordon; findlay, tristan). *J. Chem. Educ.* 1995;72(5):A109.

Spek, M. V., Banet, C., Bauer, C., Gabrielli, P., Goldthorpe, W., Mazzotti, M., et al. (2022). Perspective on the hydrogen economy as a pathway to reach net-zero CO2 emissions in Europe. *Energy Environ. Sci.* 15 (3), 1034–1077. doi:10.1039/d1ee02118d

Witman, M., Ek, G., Ling, S., Chames, J., Agarwal, S., Wong, J., et al. (2021). Data-driven discovery and synthesis of high entropy alloy hydrides with targeted thermodynamic stability. *Chem. Mat.* 33 (11), 4067–4076. doi:10.1021/acs.chemmater.1c00647

Witman, M., Ling, S., Grant, D. M., Walker, G. S., Agarwal, S., Stavila, V., et al. (2020). Extracting an empirical intermetallic hydride design principle from limited data via interpretable machine learning. *J. Phys. Chem. Lett.* 11 (1), 40–47. doi:10.1021/acs.jpclett.9b02971

Yang, X., and Zhang, Y. (2012). Prediction of high-entropy stabilized solid-solution in multi-component alloys. *Mat. Chem. Phys.* 132 (2), 233–238. doi:10.1016/j.matchemphys.2011.11.021

Zepon, G., Leiva, D. R., Strozi, R. B., Bedoch, A., Figueroa, S. J. A., Ishikawa, T. T., et al. (2018). Hydrogen-induced phase transition of MgZrTiFe0.5Co0.5Ni0.5 high entropy alloy. *Int. J. Hydrogen Energy* 43 (3), 1702–1708. doi:10.1016/j.ijhydene.2017.11.106

Zlotea, C., Chevalier-Cesar, C., Leonel, E., Leroy, E., Cuevas, F., Dibandjo, P., et al. (2011). Synthesis of small metallic Mg-based nanoparticles confined in porous carbon materials for hydrogen sorption. *Faraday Discuss.* 151, 117–131. doi:10.1039/c0fd00016g

Zlotea, C., Sow, M. A., Ek, G., Couzinié, J. P., Perrière, L., Guillot, I., et al. (2019). Hydrogen sorption in TiZrNbHfTa high entropy alloy. *J. Alloys Compd.* 775, 667–674. doi:10.1016/j.jallcom.2018.10.108

Zollinger, J., and Fleury, E. (2020). *Influence of solidification microstructure on mechanical properties of Al0.8CrCuFeNi2 high entropy alloy*. Front Mater [Internet] [cited 2022 Sep 13];7. Available from: https://www.frontiersin.org/articles/10.3389/fmats.2020.00238.